IEEE Access
Multidisciplinary | Rapid Review | Open Access Journal

Received 2 September 2024, accepted 13 September 2024, date of publication 16 September 2024,
date of current version 27 September 2024.

Digital Object Identifier 10.1109/ACCESS.2024.3462103

RESEARCH ARTICLE

An Adaptive Heart Rate Monitoring System Based on Algebraic Distance Minimization

MU LI[1,2], YANGYANG YANG[1], AND XIZHENG KE[1,2]
[1]School of Automation and Information Engineering, Xi'an University of Technology, Xi'an 710048, China
[2]Xi'an Key Laboratory of Wireless Optical Communication and Network Research, Xi'an University of Technology, Xi'an 710048, China

Corresponding author: Yangyang Yang (pubgyangyang@163.com)

This work was supported by the National Natural Science Foundation of China under Grant 61377080.

ABSTRACT A novel adaptive heart rate monitoring and filtering system based on algebraic distance minimization has been designed. This system uses frequency-modulated continuous-wave radar for non-contact monitoring of parameters such as respiration, heart rate, and heart rate variability (HRV). By employing an improved algebraic distance minimization technique, the system suppresses static noise from the environment, enhances the signal-to-noise ratio of the intermediate-frequency signal, and reduces the complexity of subsequent signal processing. To address issues such as low-frequency interference from radar signals reflecting off fixed targets around the subject and the impact of respiratory harmonics on heart rate measurement, this study introduces a respiratory harmonic filter and an adaptive notch filter to eliminate higher-order respiratory harmonic interference. This approach allows for the adaptive decomposition and reconstruction of vital sign signals and final estimation of respiratory heart rate based on the relationship between harmonics. Comparative experiments with intensive care unit medical equipment have validated the superiority and robustness of the proposed algorithm. Experimental results show that the RMSE and MRE of the method are 2.66% and 2.7%, respectively. After multiple measurements across various subjects, the method achieved an average accuracy of 96.5%, demonstrating higher measurement accuracy than other methods in all cases. Additionally, the algorithm also enables the detection of heart rate variability.

INDEX TERMS FMCW radar sensor, minimization of algebraic distance, harmonic elimination, adaptive filtering, heart rate variability.

I. INTRODUCTION

Respiratory rate and heart rate are important parameters that reflect the status of the body's signs and provide key information about the body's physiological state and health [1], [2], [3], [4]. Currently in medicine, measurements are mainly performed by electrocardiography (ECG) and photoplethysmography (PPG), however, these methods require electrodes to be glued to the chest, limbs, and other specific locations, and the measurement method is not convenient enough [5], [6]. Frequency Modulated Continuous Wave (FMCW) radar makes it easier to capture minute movements due to its high sensitivity and millimeter wavelength. Meanwhile, FMCW radar-based detection of human vital signs has the advantages of non-contact, non-invasion of privacy, and all-weather, which has become a research hotspot in recent years. [7], [8], [9], [10], [11], [12], [13], [14]. FMCW radar is more sensitive to phase information in echoes, in [15], [16], [17], [18], [19] researchers designed algorithms to extract heart rate information in the phase information part of the echo. For example, in [15], researchers proposed a peak detection algorithm for detecting vital signs, which accurately detects periodic features thus obtaining phase sequence information. The researchers in [16] chose different chirp indices from each FMCW frame structure to sample the phase variations at different sampling times and used the minimum interpolation method to obtain high resolution heartbeat signals. In [17], the researchers used the fully integrated

The associate editor coordinating the review of this manuscript and approving it for publication was Mauro Fadda.

empirical mode decomposition with adaptive noise (CEEMDAN) approach, it is concluded that human vital signs are extracted in radar phase information with high accuracy. In [20] and [21], researchers obtained high-precision heart rate respiration detection results by heart rate respiration detection in different postures. Some researchers have increased the accuracy of vital signs by improving the radar antenna based on the phase algorithm [22], [23].

Generative artificial intelligence (GAI) models have shown considerable potential in the healthcare field [24], particularly in vital signs monitoring. However, challenges related to ethics, fairness, privacy protection, and regulations cannot be overlooked [25]. Once these limitations are addressed, the future prospects for GAI in correcting misinformation and validation will be very promising [26].

When measuring respiratory heart rate by millimeter-wave radar, there are some physical interferences that can affect the accuracy of the respiratory heart rate estimation, and the most important factors are two major aspects. On the one hand, stationary targets around the detected person as well as radar transceiver antenna coupling can cause low-frequency interference. On the other hand, higher harmonics such as the second and third harmonics of respiration can interfere with the heart rate information. To overcome the above problems, researchers have improved the estimation accuracy of vital signals by varying the signal-to-noise ratio of vital signals [27], [28], [29]. In [30], [31], [32], and [33] the researchers then reduced the system DC offset as well as the static object interference signal by means of filtering to obtain a relatively pure template signal. Researchers have focused both on the elimination of respiratory high harmonics. For example, in [34], the authors designed an algorithm for heartbeat signal extraction based on Adaptive Notch Filter (ANF) and Empirical Wavelet Transform (EWT). The harmonics of respiration are suppressed, which in turn improves the heart rate information accuracy. The researchers proposed an improved fully integrated empirical mode decomposition method of phase cumulative linear interpolation combined with adaptive noise to address the effects of harmonics of respiratory signals, adaptively decomposing radar vital signs to extract heartbeat signals and estimating heart rate, in [35]. The researchers in [36] combined the variational modal decom-position (VMD) algorithm with information from the second harmonic of the heartbeat to indirectly achieve heart rate estimation by estimating the spectral peaks of the second harmonic signals, which avoids the strong interference of respiratory signals and their higher harmonics on heart rate estimation. In [37], researchers used cascaded notch filters having a respiratory harmonic controlled by the estimated fundamental respiratory frequency to eliminate respiratory harmonics, employing an adaptive algorithm to obtain robust estimates against motion artifacts and noise. To separate the respiratory and heartbeat components while maintaining signal integrity, researchers have also processed the acquired radar signals using a classical linear filtering algorithm [38], [39]. The re-searchers in [40], [41], and [42] used adaptive notch filters for filtering respiratory harmonics, which is currently a more efficient filtering method and plays a significant role in solving the problem that heart rate accuracy is easily interfered by respiratory harmonics.

The above methods contribute in signal preprocessing as well as signal decomposition as well as frequency estimation. In this paper, we propose an algebraic distance minimization (ADM) Adaptive Notch Filter (ANF) heart rate respiration system based on FMCW radar. It is a unique signal processing method to extract the signals of human body signs based on the characteristics of the complex plane and frequency domain by suppressing the low-frequency interferences of the radar system and the respiratory harmonics to the heartbeat signals at the software level. The algebraic distance minimization method processes radar intermediate frequency signals in the complex plane. First, it estimates the center offset of the signal representing the human vital signs. Then, by applying an arctangent transformation to the estimated vital sign signal's complex plane center using real-time sampled signals, it obtains the instantaneous chest displacement amplitude of the human body. Due to the nature of the arctangent function, the phase is constrained within $-\pi$ to π, requiring phase unwrapping to obtain the actual chest displacement amplitude. After the algebraic distance minimization preprocessing, to further eliminate reflections from stationary objects and the impact of respiratory harmonics on heart rate information extraction, an ANF heart rate estimation system is used to remove respiratory harmonics. The preprocessed signal is divided into I/Q signals, which are filtered by Low-Pass Filters (LPF) and Band-Pass Filters (BPF) to separate respiratory and heartbeat components. The I/Q signals are then demodulated using Complex Signal Demodulation (CSD) to combine them. Finally, an Adaptive Respiratory Harmonic Elimination Filter (RHEF) processes the respiratory frequency signal, removing higher-order harmonics of the respiratory signal, and combined with the high-pass filtered heartbeat signal, is processed by the ANF for estimation. The final heart rate is estimated based on the relationship between harmonics. After obtaining the instantaneous heart rate using the ADM-ANF algorithm, the HRV features are analyzed to assess the effectiveness and superiority of this algorithm.

II. FMCW RADAR VITAL SIGNS DETECTION PRINCIPLE

FMCW radar transmits a signal with linearly varying frequency. This signal, after being reflected by an object, is received by the radar antenna. The transmitted and the echo signals from the target are mixed and filtered, resulting in an intermediate frequency (IF) signal containing crucial distance information. Analysis of the IF signal allows for deter-mining the distance to human targets. The schematic diagram of FMCW radar transmission and reception signals, as well as the intermediate frequency (IF) signal, is shown in Fig. 1.

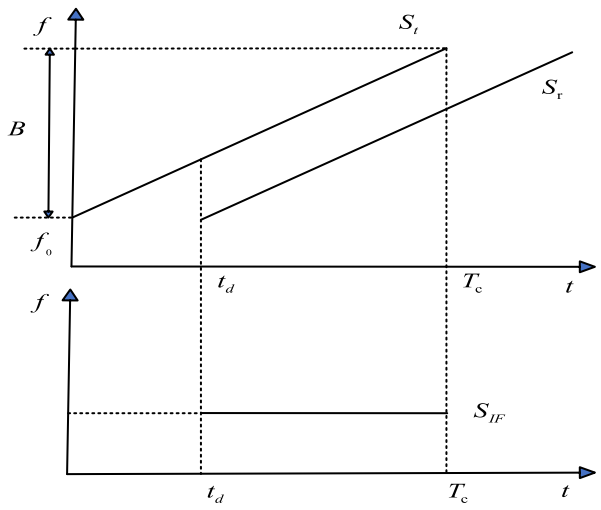

FIGURE 1. Schematic diagram of radar transceiver signal and IF signal.

The transmit signal of the FMCW radar is,

$$S_t = A_t \cos(2\pi f_0 t + \pi \frac{B}{T_c} t^2 + \Phi(t)) \tag{1}$$

where f_0 is the carrier frequency of the radar, T_c is the signal scan period, B is the bandwidth of the radar signal, A_t is the amplitude of the signal, and $\Phi(t)$ is the phase variation. The corresponding expression for the radar reflected signal is,

$$S_r = A_r \cos(2\pi f_0 (t - t_d) + \pi \frac{B}{T_c} (t - t_d)^2 + \Phi(t - t_d)) \tag{2}$$

where A_r is the amplitude of the received signal and t_d is the time delay of the signal. It is expressed as,

$$t_d = \frac{2(R + d(t))}{c} \tag{3}$$

where R is the fixed distance between the radar and the human body, d(t) is the micromotion distance from the human chest, and c is a fixed value of the speed of light. The IF signal, whose amplitude, phase and frequency are related to the distance between the human body and the radar, can be obtained by mixing the transmitted and received signals and then low-pass filtering, and the expression of the IF signal is,

$$S_{IF} = A_{IF} \cos\left[2\pi \frac{2Bd_0}{cT_c} t + \frac{4\pi d(t)}{\lambda} + \Phi(t) - \Phi(t - t_d)\right] + n(t) \tag{4}$$

where n(t) is the noise in the environment and caused by the radar itself, λ represents the wavelength of the radar.

In the measurement of small changes in chest displacement with millimeter-wave radar, the frequency change of the IF signal is very weak, but the phase change is obvious, so it is difficult to recover the motion model of the human respiratory heart rate through the processing of the amplitude and frequency information, and we mainly deal with the change of the phase in the IF signal and then extrapolated the change of the human respiratory heart rate. After deriving the simulated IF signal in order to turn it into a digital signal that can be processed by the machine we need to sample the IF signal, generally we refer to this operation as fast time sampling T_s, assuming that the total number of fast time samples is m, and in each frame we have a lot of chirps, the chirp sampling rate extracted from each frame, we refer to it as slow time sampling T_f, with the total number of samples being n. So the signal at the first sampling point in the first chirp we sample in each frame is. Fig. 2 shows the radar data sampling diagram. So the signal at the Nth sampling point in the Mth chirp we sampled in each frame is,

$$s[n, m] = A \exp(j(2\pi f_{IF} n T_f + \frac{4\pi}{\lambda} d(nT_f + mT_s))) \tag{5}$$

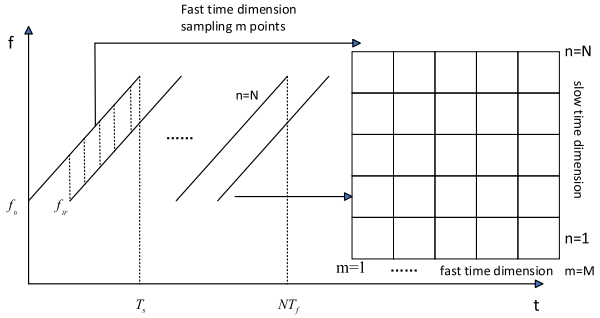

FIGURE 2. Radar data sampling.

The radar echo signal is output as an I/Q signal after quadrature mixing, the human respiration and heartbeat information is extracted through subsequent signal processing. Where the expression of the output I/Q signal is shown below,

$$I(t) = A_I \cos\left[\frac{4\pi x(t)}{\lambda} + \frac{4\pi d_0}{\lambda} + \Phi(t) - \Phi(t - \frac{2d_0}{c})\right] \tag{6}$$

$$Q(t) = A_Q \cos\left[\frac{4\pi x(t)}{\lambda} + \frac{4\pi d_0}{\lambda} + \Phi(t) - \Phi(t - \frac{2d_0}{c})\right] + \frac{\pi}{2} \tag{7}$$

III. VITAL SIGNS EXTRACTION ALGORITHM

During FMCW radar operation, the RF front-end's FMCW generator continuously produces a scanning signal with a frequency that linearly varies over time and emits it through the transmitting antenna. The electromagnetic waves radiated are reflected off the human target. The receiving antenna of the radar receives the reflected echoes from the human body. These echoes undergo orthogonal mixing with the local oscillator signal and subsequent low-pass filtering, resulting in the production of an intermediate frequency signal. However, IF signals also contain coupling from radar transceiver antennas and reflective interference from static objects around the subject, so each IF signal sampled at slow time needs to be filtered for static clutter suppression.

A. ALGEBRAIC DISTANCE MINIMIZATION ALGORITHM

In the same test scenario, other static objects caused by the clutter signal slow time to remain unchanged, and the static environment clutter amplitude is generally greater than the dynamic human body's respiratory chest undulation. The IF signal can generally be represented as follows,

$$B(t) = A_s e^{j\theta_s} + A(t)\, e^{j\frac{4\pi y(t)}{\lambda}} \tag{8}$$

The first term is the static low-frequency interference, A_s is the amplitude and θ_s is the offset and the second term is the information about the subject, A(t) is the signal strength and y(t) is the amplitude of chest rise and fall. Since static low-frequency interference is generally larger in amplitude than subject information, it can greatly interfere with the extraction of human information, an algebraic distance minimization method is introduced to reduce the effect of noise and outliers. Fig. 3 is a schematic diagram of the signal complex plane.

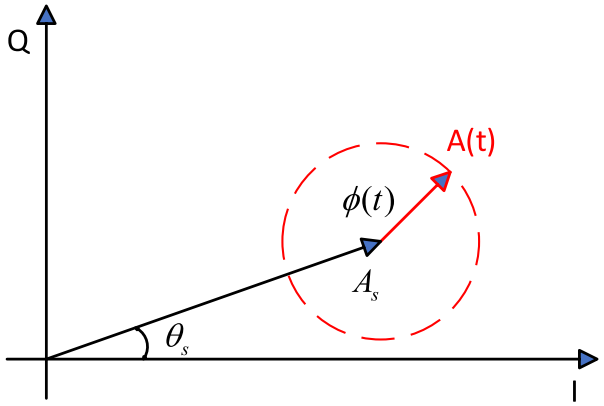

FIGURE 3. Signal complex plane schematic diagram.

In order to reduce the effect of the DC offset in the radar echo, so the Algebraic distance minimization method (ADM), or ADM processing for short, is introduced to make the circle of sign signals containing human body information in the complex plane more convergent to the origin of the complex plane. Where the general form of the circle equation is,

$$a\mathbf{x}^T\mathbf{x} + b\mathbf{x} + c = 0 \tag{9}$$

where $a \neq 0, \mathbf{b} = (b_1, b_2)$ and c are the coefficients to be computed to fit the circle from x. The above equation can be rewritten as,

$$\left(\mathbf{x_1} + \frac{b_1}{2a}\right)^2 + \left(\mathbf{x_2} + \frac{b_2}{2a}\right)^2 = \frac{||\mathbf{b}||^2}{4a^2} - \frac{c}{a} \tag{10}$$

From this the center coordinate $\mathbf{z} = (z_1, z_2)$ can be determined as respectively,

$$\mathbf{z} = (z_1, z_2) = \left(-\frac{b_1}{2a}, -\frac{b_2}{2a}\right) \tag{11}$$

The radius is determined to be,

$$r = \sqrt{\frac{||\mathbf{b}||^2}{4a^2} - \frac{c}{a}} \tag{12}$$

Therefore, a subsequent ANF heart rate respiration system can be performed to process this filtered signal, perform phase demodulation, and calculate the angle information after subtracting the center point from the I/Q signal as follows,

$$\Theta(t) = \frac{4\pi y(t)}{\lambda} = \arctan\left(\frac{\mathbf{x_2} - z_2}{\mathbf{x_1} - z_1}\right) \tag{13}$$

The results of the data before and after processing by algebraic distance minimization are shown in Fig. 4. The blue part represents the signal before processing, while the red part shows the effect after algorithm processing. It can be clearly concluded that the algorithm filters out the ambient static clutter efficiently and restores the algebraic circle containing the human body sign information to the zero point of the complex plane as much as possible.

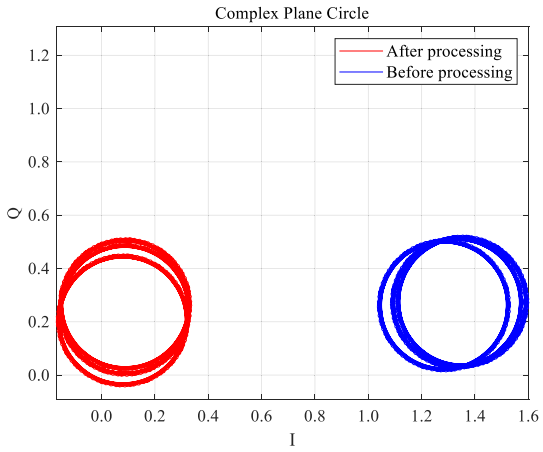

FIGURE 4. ADM algorithm processing.

Phase overlap of the sampled signals occurs when the amplitude of the human body swing is large, and in order to distinguish the chest rise and fall corresponding to different phases, it is necessary to do phase unwrapping work on the sampled signals. Performing the fast Fourier transform on the intermediate frequency signal corresponding to each chirp, the real and imaginary components of the FFT at the frequency of the spectrum's peak point are extracted. The phase-sequence waveform over time is then obtained by computing the phase using the inverse trigonometric function, arctan(I/R). Perform phase unwinding of the arctangent phases to obtain the final phase time series. The phase time series before and after unwinding are shown in Fig. 5.

B. IMPROVED ADM AND ANF ALGORITHMS FOR RESPIRATORY SIGNALING

In practical data processing, the respiration signal is easy to measure due to its low frequency and obvious amplitude,

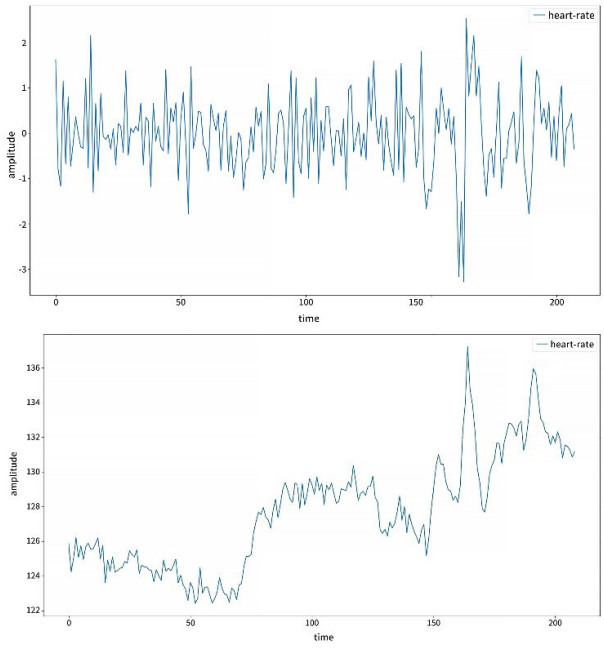

FIGURE 5. Phase time series before unwinding (above). Phase time series after unwinding (below).

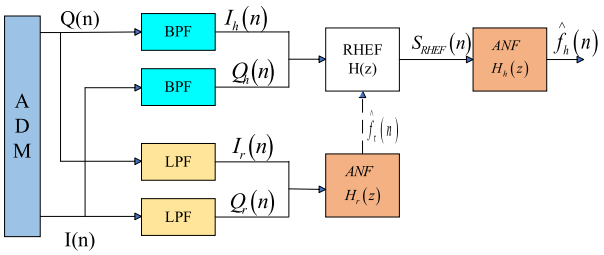

FIGURE 6. ADM-based adaptive algorithm for respiratory heart rate signaling.

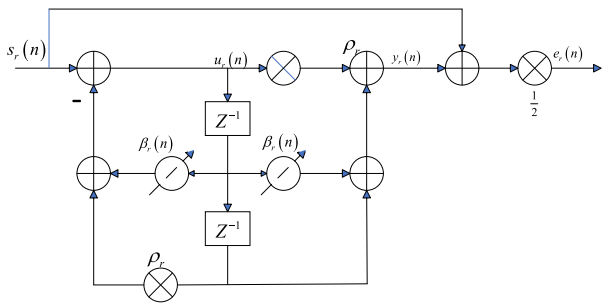

FIGURE 7. Second-order IIR filter structure.

but there are high harmonics such as second and third harmonics of respiration, which, together with the environment and the radar itself, make it more difficult to extract the heart rate information. Therefore, after filtering the IF signal, we use the ANF heart rate estimation system to eliminate the respiratory harmonics. The system comprises a bandpass filter (BPF), a low-pass filter (LPF), a complex signal demodulation (CSD) module, an adaptive notch filter ANF $H_r\,(z)$ for measuring the respiratory rate, a filter (RHEF)H(z) for removing respiratory harmonics, and an additional ANF $H_h\,(z)$ for measuring the heartbeat rate. The heart rate information is difficult to measure and will be accompanied by the interference of respiratory harmonics, so it is quite important to obtain the frequency of the respiratory signal first, the signal is processed by an algebraic distance minimization system, the filtered quadrature IF signal is passed through a low-pass filter (LPF) to obtain the desired respiratory signal for the signal processing, and then through the complex signal demodulator to the combination of quadrature signals $I_r\,(n)$ and $Q_r\,(n)$. After CSD processing the respiratory signal is obtained through the designed ANF $H_r\,(z)$ system to determine the respiratory frequency, and at the same time the real-time respiratory frequency signal is introduced into the respiratory harmonic elimination filter (RHEF)H(z) for respiratory harmonic filtration, and this filter processes the CSD-processed heart rate information and the introduced respiratory frequency signal, which is processed based on the respiratory harmonic filtration. The filtered signal is finally processed in the ANF $H_h\,(z)$ system to derive the desired heartbeat frequency. Where the data flow is shown in Fig. 6.

First, the filtered I/Q signal separates the respiratory and heartbeat components via low-pass and band-pass filters. Since the respiratory frequency is lower than the heartbeat frequency, the LPF is used to obtain the respiratory signal, and then the I/Q signals are combined by the complex signal demodulation CSD. Finally, the respiratory frequency is processed by an adaptive respiratory notch filter. The respiratory filter $H_r\,(z)$ contains a second-order IIR filter with all-pass filter characteristics. structure illustrated in Fig. 7 [37].

The transfer function of the system is,

$$H_r\,(z) = \frac{1}{2}\frac{(1+\rho_r) + 2\rho_r\,(n)\,z^{-1} + (1+\rho_r)\,z^{-2}}{1 + \beta_r\,(n)\,z^{-1} + \rho_r z^{-2}} \tag{14}$$

where ρ_r is the squared pole radius of $H_r\,(z)$ with a magnitude of 0.96, $\beta_{\mathrm{r}}\,(\mathrm{n})$ is the estimated respiratory frequency correlation coefficient, and the control amplitude response $H_r\,(z)$ becomes zero, where $\beta_{\mathrm{r}}\,(0)$ is set to 18, The complex normalized mini-mum mean square algorithm is utilized to vary the tap coefficient $\beta_{\mathrm{r}}\,(\mathrm{n})$. which is implemented as,

$$\begin{aligned}&\beta_r\,(n+1)\\ &= -\,(1+\rho_r)\cos 2\pi\left(\frac{f_r\,(n)}{F_s}\right) - u_r\frac{e_r\,(n)\,u_r^*\,(n-1)}{u_r^2\,(n-1)}\end{aligned} \tag{15}$$

where F_s is the sampling frequency, $u_r\,(n)$ is the tapped input signal to the second or-der IIR filter. u_r is the step value of 0.05 and * denotes conjugate. Since the fundamental wave of respiration occupies $s_r\,(n)$, the frequency of respiration is estimated as the notch frequency. The estimated respiratory rate $\hat{f}_r\,(n)$ is given by the following equation,

$$\hat{f}_r\,(n) = \frac{F_s}{2\pi}\cos^{-1}\left\{-\frac{\beta_r\,(n)}{1+\rho_r}\right\} \tag{16}$$

C. RESPIRATORY HARMONIC FILTER AND HEART RATE ESTIMATION

Due to the large amplitude of the second and third harmonics of the respiratory signal, especially the third resonance can interfere with the extraction of the heart rate information, a respiratory harmonic filter, RHEF H_r (z), was designed, which consists of cascaded notch filters. However, more orders of notch filter settings would make the notch bandwidth too wide to reduce harmonics, so two orders are set. In addition, the estimated respiration frequency $\hat{f}_r(n)$ determines the notch frequency, with its transfer function provided by the following equation,

$$H(z) = \prod_{m=1}^{2} \frac{1}{2} \frac{(1+\rho) + 2\beta_m(n) z^{-1} + (1+\rho) z^{-2}}{1 + \beta_m(n) z^{-1} + \rho z^{-2}} \quad (17)$$

where ρ denotes the square of the pole radius set to 0.98, and β_m is the tap coefficient corresponding to the (m+1)th harmonic frequency of the breath. $\beta_m(n)$ denotes the,

$$\beta_m(n) = -(1+\rho) \cos\left\{2\pi \frac{(m+1)\hat{f}_r(n)}{F_s}\right\} \quad (18)$$

Based on the estimated respiratory rate $\hat{f}_r(n)$, the notch frequency of H(z) varies. Therefore, as the resulting output signal of H(z), the proposed system can acquire the signal that reduces the respiratory harmonics that interfere with the heartbeat component. The narrow notch band of the notch filter is effectively preserved by the RHEF, thereby reducing the loss of the heartbeat component. The transfer function $H_h(z)$ of heart rate is denoted as,

$$H_h(z) = \frac{1}{2} \frac{(1+\rho_h) + 2\beta_h(n) z^{-1} + (1+\rho_h) z^{-2}}{1 + \beta_h(n) z^{-1} + \rho_h z^{-2}} \quad (19)$$

where ρ_h is the radius of the square pole of $H_h(z)$ and has size 0.96, β_h (n) is the estimated heart rate correlation coefficient controlling for the magnitude response H_h (z) becomes zero, where β_h (0) is 115 and the tap coefficient is changed using the following complex normalized least mean square (NLMS) algorithm, the specific formula is realized as follows,

$$\beta_h(n+1) = -(1+\rho_h) \cos 2\pi \left(\frac{f_h(n)}{F_s}\right) - u_h \frac{e_h(n) u_h^*(n-1)}{u_h^2(n-1)} \quad (20)$$

where F_s represents the sampling frequency and $u_h(n)$ represents the tapped input signal of the second-order IIR filter. u_h denotes a step value of 0.1 and * denotes the con-jugate. Based on the notch frequency and the tap coefficient $\beta_h(n)$, the estimated heart rate $\hat{f}_h(n)$ is defined as,

$$\hat{f}_h(n) = \frac{F_s}{2\pi} \cos^{-1}\left\{-\frac{\beta_h(n)}{1+\rho_h}\right\} \quad (21)$$

Based on the above analysis, we propose an algebraic distance minimization ANF heart rate respiration system based on FMCW radar, the data flow diagram is shown in Fig. 8. The signal processing algorithm consists of three parts by suppressing the effects of stationary targets around the detected person as well as low-frequency interference caused by the radar transceiver antenna coupling, and respiratory harmonics on the heartbeat signal at the software level. The radar IF signal is first processed by an algebraic distance minimization algorithm to filter out the low frequency offset of the radar system and the environmental static clutter signal, and the processed orthogonal body signals are processed in the designed ANF heart rate respiration system. Next, the respiratory and heartbeat signals are filtered by the designed low-pass filter and high-pass filter, respectively, where the respiratory signal is estimated by the designed respiratory filter ANF. Finally, the real-time respiratory frequency signal is introduced into the respiratory harmonic elimination filter RHEF to filter out the higher harmonics of the respiratory signal, and combined with the high-pass filtered heartbeat signal, Estimation was performed by an adaptive heart rate filter ANF based on filtering out the respiratory high harmonics, and final estimation of the respiratory heart rate was performed by analyzing the relationship between the harmonics.

D. HEART RATE VARIABILITY

Heart Rate Variability (HRV) is the natural fluctuation in the time interval between heartbeats over a period of time. It can measure the degree of variability between heart-beats and can reflect a variety of important physiological indicators of cardiovascular health, autonomic nervous system function, and stress and recovery levels [43], [44].

Different from the direct detection of the time interval of neighboring heartbeats in the heartbeat signal in the time domain. In this paper, we improve the ADM-ANF algorithm to obtain more accurate frequency domain signals, and by calculating the peak frequency of the heartbeat signal, we get the consecutive heartbeat interval period, which is ex-pressed by Beat-to-Beat Interval (BBI) as shown in equation (22),

$$BBI(i) = \left(60 \Big/ \frac{60}{f_0}\right) \times 1000, i = 1, 2, \ldots, N \quad (22)$$

By substituting the successive heartbeat intervals BBI into equations (25), (26), and (27), the characteristic parameters of HRV can be derived, which are clinically significant, as shown in Table 1.

Detection of HRV has been widely used in clinical practice to predict coronary heart disease, myocardial infarction, hypertension, cardiac insufficiency, and other diseases with phycological dysfunction. Non-contact detection of HRV by radar is of great value in the prediction of related diseases [45].

In this paper, the human heart rate signal is extracted by the proposed ADM-ANF separation algorithm, then the human instantaneous heart rate is extracted by the adaptive heart rate trap filter, and finally the HRV is analyzed by calculating the eigenvalues of HRV.

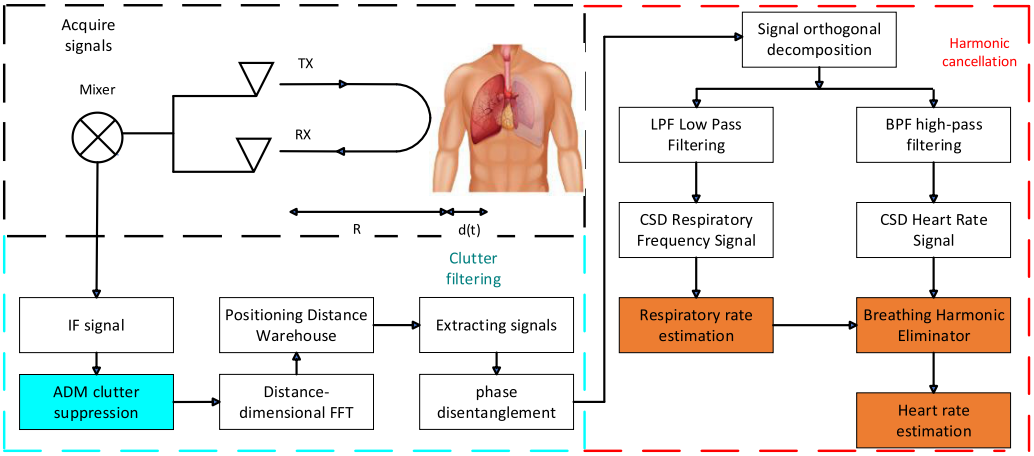

FIGURE 8. Signal processing flow chart.

TABLE 1. HRV parameters and their significance.

parameters	descriptive	reference value /ms	Abnormal range/ms	abnormal significance
$Mean_{RR}$	mean value of RR interval	600~1000	>1000	Tachycardia
SDNN	Standard deviation of the NN interval	100~150	<50	Dcreased sympathetic activity
RMSSD	Root mean square of the difference between nei ghboring NN intervals	20~50	<20	Decreased parasympathetic activity

IV. EXPERIMENTAL RESULTS AND ALGORITHM DESIGN

A. DEVICE SELECTION

In this paper, Texas Instruments' IWR1843 millimeter wave radar with DCA1000 data acquisition card is used to capture the micro-motion signals from the human anterior chest wall, and the device is shown in Fig. 9. IWR1843 radar works in the frequency band of 77∼81GHz, 77GHz FMCW radar bandwidth has 4GHz has a high distance resolution, can realize the linear FM signal transmission, reception and IF signal sampling, DCA1000 Data Acquisition Card is the IF signal through the Ethernet interface to the up-per computer, the radar parameters as shown in Table 2. Fig. 9(a) shows a physical drawing of the radar, Fig. 9(b) shows the antenna distribution, and Fig. 9(c) shows the DAC1000 acquisition data board. The DAC1000 data acquisition board samples the received signals and sends the data to a computer. The computer, using a serial port tool within a QT visualization interface, receives and processes the data. The chest, respiratory, and heart rate waveform graphs are displayed in real-time, and the recorded data is analyzed and processed in matlab. Fig. 9(d) shows the experimental environment. All experiments appearing in this paper have received informed consent from the subjects.

According to the Nyquist Sampling Theorem, to retain full heart rate data, the chirp repetition rate must exceed twice the highest heart rate. According to medical statistics, the heart rate of an average individual is typically between 60-90 beats per minute. In light of this, we opted to establish a 50-millisecond interval for the radar's chirp repetition period,

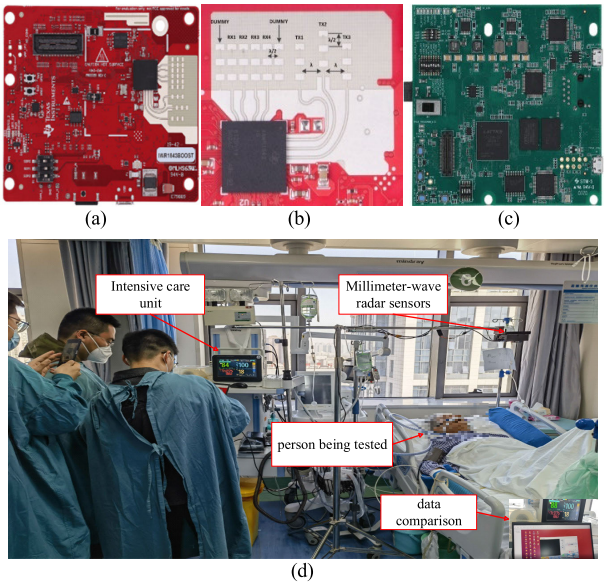

FIGURE 9. (a) Physical diagram of IWR1843 (b) Radar antenna distribution (c) DAC1000 data acquisition board (d) Experimental environment diagram.

TABLE 2. Parameter settings of the radar.

Parameters	Value
Starting frequency /GHz	77
Chirp slope(MHz/μs)	70
Bandwidth/GHz	4
Frame rate	1024
Frame period/ms	50
Number of chirps per frame	2
ADC sampling rate /ksps	4000
Chirp duration/us	50

coupled with a sampling frequency of 20 Hz, to meet the operational needs.

B. OPTIMIZATION ALGORITHM COMPARISON EXPERIMENT

Ant Colony Optimization (ACO) [46] and Genetic Algorithms (GA) [47] are commonly used optimization algorithms, widely applied in function optimization and neural network training. To validate the superiority of the ADM shrinkage algorithm in terms of convergence speed and optimal performance, a comparative experiment with the above three algorithms was conducted. Fig. 10 shows the fitness evolution curves of the three optimization algorithms.

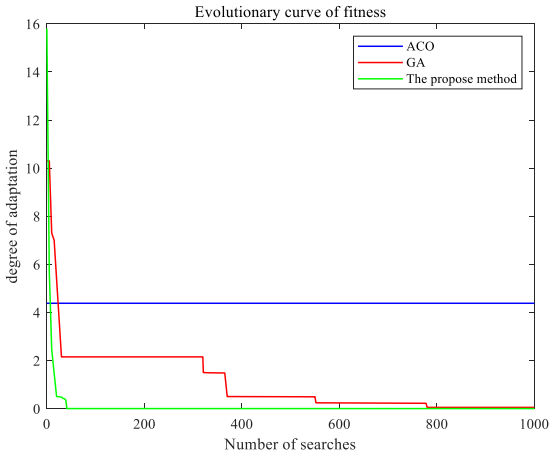

FIGURE 10. The fitness evolution curves of the three algorithms.

From the experimental results in Fig. 10, it can be observed that ACO falls into a local optimum early in the iteration, performing the worst. Particle Swarm Optimization (PSO) approaches the optimal solution after continuous iterations but is slower. In contrast, the ADM shrinkage algorithm used in this paper excels in accuracy, convergence speed, and performance, with experimental results confirming its superiority in the life sign separation algorithm.

C. MEASUREMENT EXPERIMENTS AND ERROR ANALYSIS

In order to reduce the influence of radar system low frequency interference on detection results, we first test the algebraic distance minimization method, different from the previous complex plane experiments, in order to be able to visualize and compare the filtering effect, we chose to analyze the collected original thoracic undulation signals in the frequency domain which includes the thoracic undulation map as shown in Fig. 11(a), and its corresponding signal in the frequency domain is shown in Fig. 11(b), where f_{SC} represents the low frequency offset interference suffered by the radar system, f_{RR} and f_{HR} represent the respiratory and heart rate frequencies of the subject, respectively, while $2f_{RR}$ and $3f_{RR}$ in the middle represent the second and third harmonics of the respiratory signal, respectively. From Fig. 11 it can be clearly concluded that the low frequency offset of the radar system interferes with the human body signals, By means of ADM method, we process the collected continuous signals in the complex plane region, eliminate the relatively large static low-frequency com-ponents in the signals, and enhance the signal-to-noise ratio of human body signs, and we have observed the results in the frequency domain after the processing through the ADM method. Fig. 11(c) shows the chest undulation map after ADM processing, Fig. 11(d) shows the frequency domain signal of the chest cavity after ADM processing. It can be seen that the proportion of static clutter in the echo signal is greatly reduced and the signal-to-noise ratio of the echo signal is substantially improved.

At each measurement, the fast Fourier (FFT) transform is performed on the ADC data to obtain the Rang curve, and through the approximate positional relationship between the radar and the human body, the distance range of the target can be determined, and the maximum value is searched for within the range to obtain the distance bin corresponding to the target (Range bin), and the phase of the target is extracted once in each frame period, and the cyclic launch of N frames will obtain the target phase with the number of frames of the value of the target, and get the target phase vs. time, and it can be regarded as vibration signals as well, as shown in Fig. 12(a). The complex baseband signals are extracted in the bins corresponding to the chest position, and are filtered for the first time by the algebraic distance minimization method to remove the influence of the DC offset in the environment, and the filtered orthogonal signals are low-pass filtered as well as high-pass filtered, and the low-pass filtered orthogonal signals filtered by the complex signal de-modulation CSD combination. Then the respiratory rate is determined by the adaptive ANF respiratory estimation system $H_r(z)$. The heartbeat signal is band-pass filtered and then the signal is passed through the respiratory harmonic eliminator RHEF to remove the high harmonics of respiration, and finally the heartbeat rate is determined by the ANF heart rate estimation system $H_h(z)$.

To better reflect the performance of the proposed method, the subjects intentionally increased the amplitude and frequency of breathing to increase the effect of respiratory harmonics on heart rate. Fig. 12 shows the experimental results of a set of measurements.

Fig. 12(a) shows the thoracic amplitude map of the original signal, and Fig. 12(b) shows the corresponding spectrogram

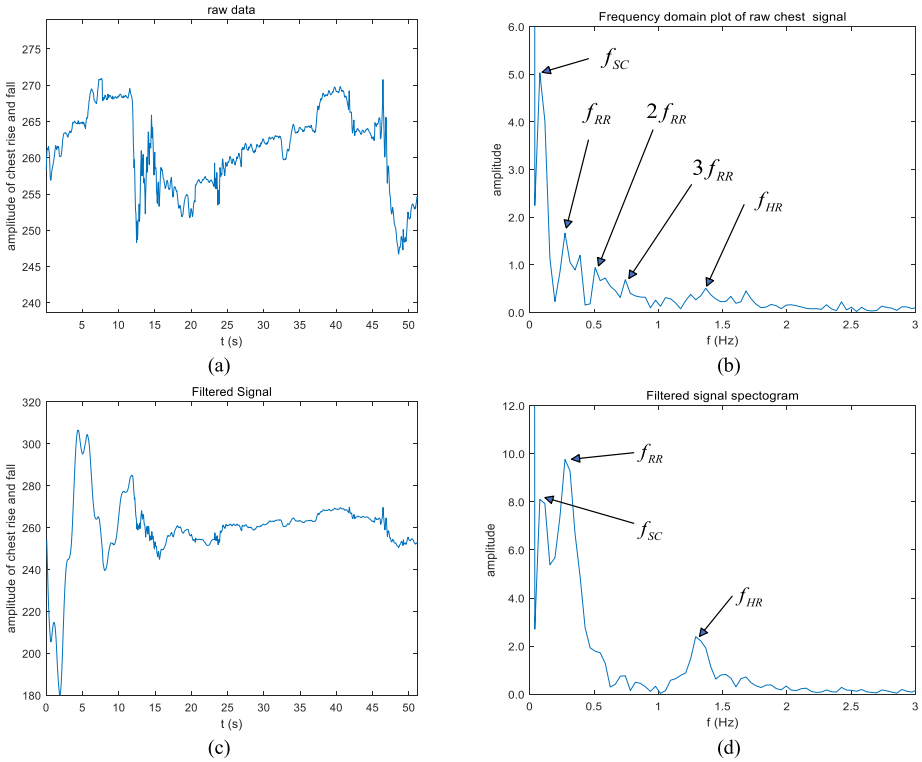

FIGURE 11. (a) Physical diagram of IWR1843 (b) Radar antenna distribution (c) DAC1000 data acquisition board (d) Experimental environment diagram.

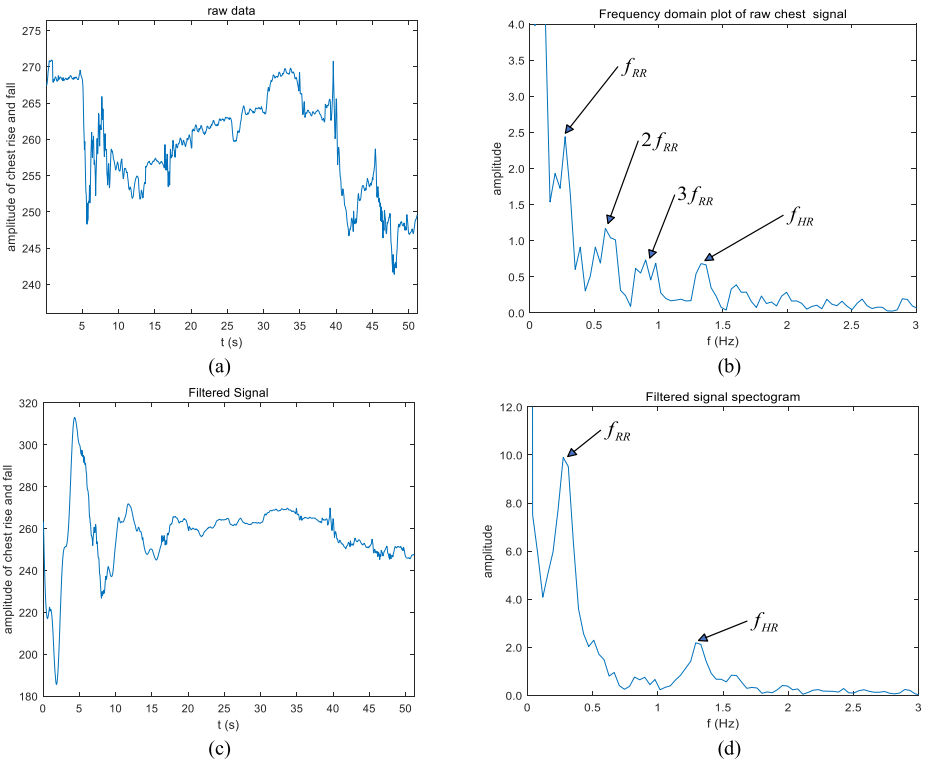

FIGURE 12. (a) Raw data magnitude plot (b) Raw data frequency domain plot (c) Filtered data magnitude plot (d) Filtered data frequency domain plot.

of the original signal, it can be seen that the second and third harmonics of the respiration are very obvious, and even the third harmonic amplitude is slightly larger than the heart rate information, which may be recognized as the heart rate information, which has a large impact on the extraction of the heart rate information, and its impact can be reduced by the method proposed in this study. Fig. 12(d) shows the spectrogram after filtering with the proposed method. It can be seen that the high harmonics of respiration are effectively filtered out from the filtered frequency map, and the frequency peaks of respiration and heart rate are significantly improved after filtering, which makes it easier to extract the information of respiration and heart rate.

The next work focuses on evaluating the accuracy of the heart rate information estimates. We compared the test data with the data from the intensive care unit equipment. Each measurement of 1024 data corresponded to a measurement time of 51.2 seconds. We measured radar data from 6 subjects (p1-p6) of different body types and ages. The subjects maintained normal respiration during the testing process, with measurements conducted for 300 seconds at distances of 0.5 meters and 1 meter. During testing, 1024 continuous phase data points were extracted and processed using the algorithm proposed in this paper. The experimental environment was arranged as shown in Fig. 9(d). Fig. 13 shows the results of measuring HR and RR with different methods.

The method gives more accurate results compared to the other three methods. The results presented in Fig. 13 validate that the proposed method achieves superior overall performance compared to other methods, which proves the accuracy of the method based on minimizing the ANF respiratory heart rate system over algebraic distance in heartbeat estimation. The average relative error of the method is reduced to 2.7% when compared with the other three methods.

To better evaluate the algorithm's advantages, this paper employs Mean Relative Error (MRE) and Root Mean Square Error (RMSE) to quantify the accuracy of different methods, respectively represented as,

$$RMSE = \sqrt{\frac{1}{N}\sum_{i=1}^{N}\left(HR_{ref}\,[i] - HR_{meas}\,[i]\right)^2} \tag{23}$$

$$MRE = \frac{1}{N}\sum_{i=1}^{N}\frac{\left|HR_{ref}\,[i] - HR_{meas}\,[i]\right|}{HR_{ref}\,[i]} \tag{24}$$

where N is the number of test data, HR_{ref} is the heart rate reference value, and HR_{meas} is the heart rate estimate for the proposed method. Table 3 shows the heart rate data collected from six volunteers and the errors.

Considering the differences in environmental conditions between daily and medical monitoring, distance factors may impact experimental data. This paper conducted experiments at distances of 0.5 meters and 1 meter to validate the influence of distance on radar-based vital signs detection. Table 4 presents the evaluation of heart rate detection results under these different distance conditions.

TABLE 3. Experimental errors of different methods.

arithmetic	RMSE	MRE
VMD	6.11 bpm	6.4%
Peak Detection	4.26bpm	5.1%
CEEMDAN	3.43bpm	4.2%
EWT	9.40bpm	9.4%
MCM	7.27bpm	7.6%
OPF	5.27bpm	5.7%
The propose method	2.66bpm	2.7%

TABLE 4. Measurement data and errors for different distances and testers.

Distance	0.5m			1.0m		
Subject	HR Accuracy	RMSE HR (BPM)	MRE HR (BPM)	HR Accuracy	RMSE HR (BPM)	MRE HR (BPM)
P1	96.7%	2.07	2.19	93.8%	3.65	2.72
P2	98.2%	2.27	2.63	96.5%	2.70	3.26
P3	98.1%	2.45	2.57	97.6%	2.66	2.89
P4	96.7%	2.58	2.39	93.5%	2.75	2.65
P5	96.9%	2.59	2.44	94.6%	2.76	2.56
P6	94.6%	2.48	2.38	92.7%	2.33	2.38

From the results in Table 4, it can be seen that the detection of human heart rate by the radar at distances of 0.5 meters and 1 meter did not show significant differences, both demonstrating high accuracy. The results also indicate the high precision of the vital sign detection algorithm proposed in this paper within a certain distance range.

D. HEART RTE VARIABILITY EXPERIMENT

The article utilizes the proposed ADM-ANF separation algorithm to extract the hu-man heart rate signal, and subsequently employs an adaptive heart rate notch filter to ex-tract the instantaneous heart rate. Finally, experiments were conducted on HRV, and comparisons were made with an ECG sensor. Ten sets of experimental data were selected to calculate the HRV intervals. Fig. 14 displays experimental scenarios comparing HRV, while Fig. 15 presents a line graph comparing the experimental data.

From the above experimental results, it is evident that the heart rate intervals obtained by the algorithm proposed in this article are closer to the ECG signal. In contrast, the CEEMDAN, VMD, and Peak Detection algorithms exhibit errors in heart rate signal extraction, leading to larger discrepancies in heart rate interval calculations.

The article evaluates the effectiveness and superiority of the proposed algorithm's experimental data using three HRV feature indices. Among these, Standard Deviation of NN Intervals (SDNN) and Root Mean Square of the Successive Differences (RMSSD) are critical metrics for assessing HRV [1]. They play a significant role in predicting cardiac diseases. Their increase or decrease directly impacts HRV analysis.

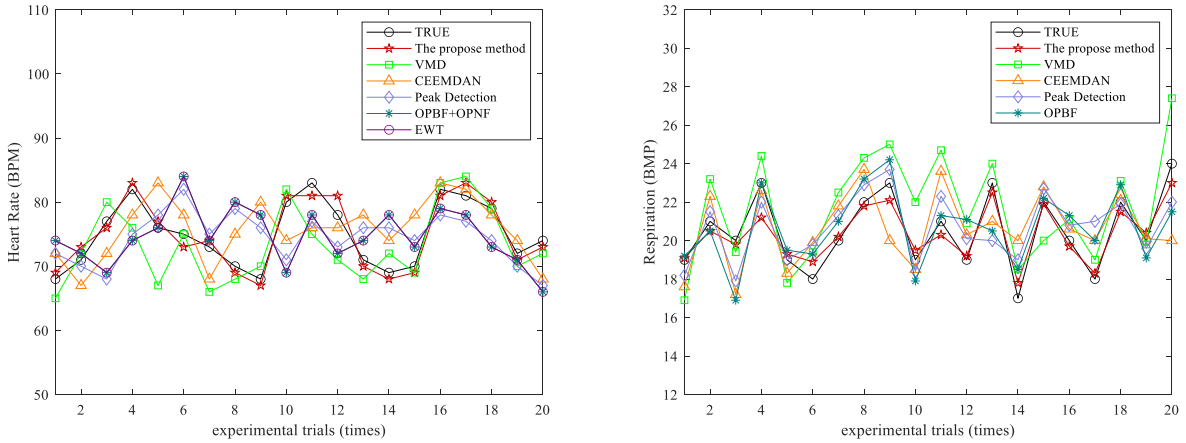

FIGURE 13. Heart rate and respiration detection comparison experiment.

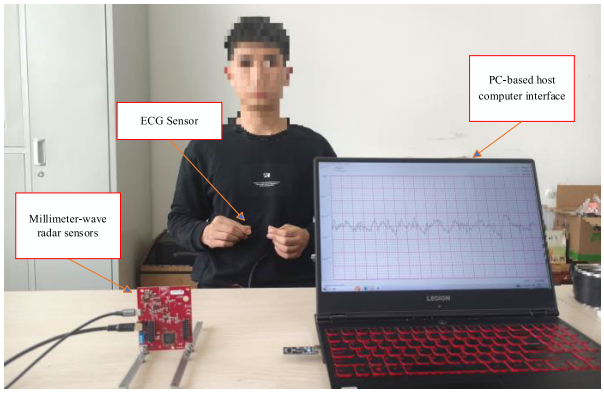

FIGURE 14. Scenario diagram of the HRV comparison experiment.

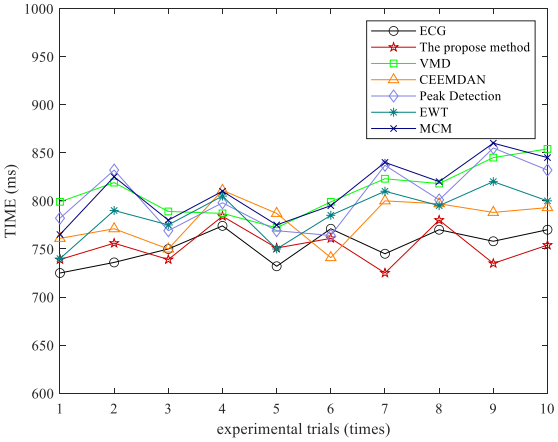

FIGURE 15. Comparison of experimental data on cardiac interval cycles.

The Mean of the R-R Intervals ($Mean_{RR}$), refer to "(25),"

$$V_{Mean_{RR}} = \sum_{i=1}^{N_{BBI}} \frac{RR_i}{N_{BBI}} \tag{25}$$

The standard deviation of RR intervals (SDNN), refer to "(26),"

$$V_{SDNN} = \sqrt{\frac{1}{N_{BBI}} \sum_{i=1}^{N_{BBI}} \left(RR_i - \overline{RR}\right)^2} \tag{26}$$

The root mean square of successive differences of NN intervals (RMSSD), refer to "(27),"

$$V_{RMSSD} = \sqrt{\frac{1}{N_{BBI} - 1} \sum_{i=1}^{N_{BBI}} (RR_{i+1} - RR_i)^2} \tag{27}$$

N_{BBI} represents the number of normal RR intervals. $\overline{RR}$ represents the average value of normal RR intervals over the entire segment.

Considering the errors in the RR interval mean values obtained by the algorithm proposed in this article, CEEMDAN, and Peak Detection algorithms compared to the actual values detected by the ECG device, there is misleading information in the calculation of SDNN using Equation (25). Therefore, in the calculation, replacing $\overline{RR}$ with the corresponding accurate values from the ECG device over the same experimental duration as $\overline{RR}$ better illustrates the performance of the three algorithms compared to the ECG device. Table 5 presents the comparison of HRV feature values.

Based on the results from the above table, the algorithm proposed in this paper shows a difference of only 6.7 in the mean RR interval compared to the ECG device. The standard deviation of RR intervals and the difference between NN intervals are higher than the CEEMDAN algorithm by 30.14 and 23.88, respectively, higher than the Peak Detection algorithm by 3.93 and 22.19, respectively, higher than the VMD algorithm by 20.61 and 8.05, higher than the EWT algorithm by 13.48 and 15.30, and higher than the MCM algorithm by 23.73 and 21.17, respectively. The experimental results demonstrate the effectiveness and superiority of the proposed algorithm in HRV detection.

TABLE 5. Comparison of HRV eigenvalues.

arithmetic	$Mean_{RR}$	SDNN	RMSSD
ECG	753.1	24.95	20.92
The propose method	746.4	33.75	17.64
CEEMDAN	830.5	63.89	41.52
Peak Detection	789.9	37.68	39.83
VMD	809.9	54.36	25.69
EWT	790.0	47.23	32.94
MCM	812.5	57.48	38.81

V. CONCLUSION

In this study, in order to extract the frequency information of respiration and heart-beat during micro-movements of the human chest wall, this paper establishes a millimeter-wave radar vital sign signal model and proposes an ANF respiration heart rate extraction method based on algebraic distance minimization. The traditional method will reduce the estimation accuracy due to the low-frequency offset interference of the radar system and the presence of respiratory harmonics. The proposed method will extract the complex baseband signal from the corresponding distance bin of the subject's chest, filter it for the first time by algebraic distance minimization method, and then filter the respiratory harmonics by ANF respiratory heart rate system, and finally estimate the heart rate information. Two scenarios were tested and studied on six human subjects at different distances. In each experiment, to ensure data validity, 1024 data samples in steady state were taken for processing each time, which corresponded to a monitoring time of 51.2s to prevent chance errors.

The results of human experiments show that the proposed method can effectively converge the signals containing the human body signs information to the zero point of the complex plane, which reduces the impact of the radar system due to the low-frequency interference. The signal after minimizing the algebraic distance is processed in the ANF respiratory heart rate system, which effectively extracts the respiratory signal and reduces the influence of respiratory harmonics on the heart rate information, improving the accuracy of the heart rate information. By using the FMCW sensor and the proposed processing algorithm, the average accuracy of the estimation of the respiration rate and the heart rate is not less than 96.5%.

REFERENCES

[1] H. Xu, M. P. Ebrahim, K. Hasan, F. Heydari, P. Howley, and M. R. Yuce, "Accurate heart rate and respiration rate detection based on a higher-order harmonics peak selection method using radar non-contact sensors," *Sensors*, vol. 22, no. 1, p. 83, Dec. 2021, doi: 10.3390/s22010083.

[2] K. Higashi, G. Sun, and K. Ishibashi, "Precise heart rate measurement using non-contact Doppler radar assisted by machine-learning-based sleep posture estimation," in *Proc. 41st Annu. Int. Conf. IEEE Eng. Med. Biol. Soc. (EMBC)*. Germany: IEEE, Jul. 2019, pp. 788–791, doi: 10.1109/EMBC.2019.8857830.

[3] G. Sun, Y. Tanaka, K. Kiyono, K. Hashimoto, B. Takase, H. Liu, T. Kirimoto, and T. Matsui, "Non-contact monitoring of heart rate variability using medical radar for the evaluation of dynamic changes in autonomic nervous activity during a head-up tilt test," *J. Med. Eng. Technol.*, vol. 43, no. 7, pp. 411–417, Oct. 2019, doi: 10.1080/03091902.2019.1687771.

[4] S. M. M. Islam, "Radar-based remote physiological sensing: Progress, challenges, and opportunities," *Frontiers Physiol.*, vol. 13, Oct. 2022, Art. no. 955208, doi: 10.3389/fphys.2022.955208.

[5] K. Edanami and G. Sun, "Medical radar signal dataset for non-contact respiration and heart rate measurement," *Data Brief*, vol. 40, Feb. 2022, Art. no. 107724, doi: 10.1016/j.dib.2021.107724.

[6] K. Edanami, Y. Yao, H. T. Yen, M. Kurosawa, T. Kirimoto, Y. Hakozaki, T. Matsui, and G. Sun, "Design and evaluation of digital filters for non-contact measuring of HRV using medical radar and its application in bedside patient monitoring system," in *Proc. 43rd Annu. Int. Conf. IEEE Eng. Med. Biol. Soc. (EMBC)*. Mexico: IEEE, Nov. 2021, pp. 6962–6965, doi: 10.1109/EMBC46164.2021.9629643.

[7] C. Gouveia, D. F. Albuquerque, P. Pinho, and J. Vieira, "Bio-radar cardiac signal model used for HRV assessment and evaluation using adaptive filtering," *IEEE Trans. Instrum. Meas.*, vol. 71, pp. 1–10, 2022, doi: 10.1109/TIM.2022.3190035.

[8] M. Giordano, G. Islamoglu, V. Potocnik, C. Vogt, and M. Magno, "Survey, analysis and comparison of radar technologies for embedded vital sign monitoring," in *Proc. 44th Annu. Int. Conf. IEEE Eng. Med. Biol. Soc. (EMBC)*, Jul. 2022, pp. 854–860, doi: 10.1109/EMBC48229.2022.9871847.

[9] J. N. Sameera, A. D. Droitcour, and O. Boric-Lubecke, "Heart rate detection using single-channel Doppler radar system," in *Proc. 44th Annu. Int. Conf. IEEE Eng. Med. Biol. Soc. (EMBC)*. United Kingdom: IEEE, Jul. 2022, pp. 1953–1956, doi: 10.1109/EMBC48229.2022.9871199.

[10] M. Alizadeh, G. Shaker, J. C. M. D. Almeida, P. P. Morita, and S. Safavi-Naeini, "Remote monitoring of human vital signs using mm-wave FMCW radar," *IEEE Access*, vol. 7, pp. 54958–54968, 2019, doi: 10.1109/ACCESS.2019.2912956.

[11] V. L. Petrovic, M. M. Jankovic, A. V. Lupsic, V. R. Mihajlovic, and J. S. Popovic-Božovic, "High-accuracy real-time monitoring of heart rate variability using 24 GHz continuous-wave Doppler radar," *IEEE Access*, vol. 7, pp. 74721–74733, 2019, doi: 10.1109/ACCESS.2019.2921240.

[12] E. Turppa, J. M. Kortelainen, O. Antropov, and T. Kiuru, "Vital sign monitoring using FMCW radar in various sleeping scenarios," *Sensors*, vol. 20, no. 22, p. 6505, Nov. 2020, doi: 10.3390/s20226505.

[13] K. Gupta, O. J. Pandey, and L. R. Cenkeramaddi, "Automatic contactless monitoring of breathing rate and heart rate utilizing the fusion of mmWave radar and camera steering system," *IEEE Sensors J.*, vol. 22, no. 22, pp. 22179–22191, Nov. 2022, doi: 10.1109/JSEN.2022.3210256.

[14] Y. Hu and T. Toda, "Remote vital signs measurement of indoor walking persons using mm-wave FMCW radar," *IEEE Access*, vol. 10, pp. 78219–78230, 2022, doi: 10.1109/ACCESS.2022.3193789.

[15] J.-Y. Kim, J.-H. Park, S.-Y. Jang, and J.-R. Yang, "Peak detection algorithm for vital sign detection using Doppler radar sensors," *Sensors*, vol. 19, no. 7, p. 1575, Apr. 2019, doi: 10.3390/s19071575.

[16] D. Jung, S. Cheon, D. Kim, J. Yoon, and B. Kim, "Short time remote heart rate measurement based on mmWave FMCW radar frame structure," *IEEE Antennas Wireless Propag. Lett.*, vol. 22, no. 6, pp. 1–5, Jun. 2023, doi: 10.1109/LAWP.2023.3241153.

[17] J. Guo, Y. Bian, W. Wang, H. Dai, and J. Chen, "Respiration and heart rates measurement using 77GHz FMCW radar with blind source separation algorithm," in *Proc. 44th Annu. Int. Conf. IEEE Eng. Med. Biol. Soc. (EMBC)*, vol. 67. United Kingdom: IEEE, Jul. 2022, pp. 842–845, doi: 10.1109/embc48229.2022.9871987.

[18] F. Michler, K. Shi, S. Schellenberger, T. Steigleder, A. Malessa, L. Hameyer, N. Neumann, F. Lurz, C. Ostgathe, R. Weigel, and A. Koelpin, "A clinically evaluated interferometric continuous-wave radar system for the contactless measurement of human vital parameters," *Sensors*, vol. 19, no. 11, p. 2492, May 2019, doi: 10.3390/s19112492.

[19] S. Iyer, L. Zhao, M. P. Mohan, J. Jimeno, M. Y. Siyal, A. Alphones, and M. F. Karim, "Mm-wave radar-based vital signs monitoring and arrhythmia detection using machine learning," *Sensors*, vol. 22, no. 9, p. 3106, Apr. 2022, doi: 10.3390/s22093106.

[20] J. Wu and N. Dahnoun, "A health monitoring system with posture estimation and heart rate detection based on millimeter-wave radar," *Microprocessors Microsystems*, vol. 94, Oct. 2022, Art. no. 104670, doi: 10.1016/j.micpro.2022.104670.

[21] Y.-C. Tsai, S.-H. Lai, C.-J. Ho, F.-M. Wu, L. Henrickson, C.-C. Wei, I. Chen, V. Wu, and J. Chen, "High accuracy respiration and heart rate detection based on artificial neural network regression," in *Proc. 42nd Annu. Int. Conf. IEEE Eng. Med. Biol. Soc. (EMBC)*. QC, Canada: IEEE, Jul. 2020, pp. 232–235, doi: 10.1109/embc44109.2020.9175161.

[22] J. Xiong, H. Hong, L. Xiao, E. Wang, and X. Zhu, "Vital signs detection with difference beamforming and orthogonal projection filter based on SIMO-FMCW radar," *IEEE Trans. Microw. Theory Techn.*, vol. 71, no. 1, pp. 83–92, Jan. 2023, doi: 10.1109/TMTT.2022.3181129.

[23] S. Ahmed, J. Park, and S. H. Cho, "Effects of receiver beamforming for vital sign measurements using FMCW radar at various distances and angles," *Sensors*, vol. 22, no. 18, p. 6877, Sep. 2022, doi: 10.3390/s22186877.

[24] Y. Derbal, "Adaptive cancer therapy in the age of generative artificial intelligence," *Cancer Control*, vol. 31, Jan. 2024, Art. no. 10732748241264704, doi: 10.1177/10732748241264704.

[25] M. O. Tamam and M. C. Tamam, "Artificial intelligence technologies in nuclear medicine," *World J. Radiol.*, vol. 14, no. 6, pp. 151–154, Jun. 2022, doi: 10.4329/wjr.v14.i6.151.

[26] S. Reddy, "Generative AI in healthcare: An implementation science informed translational path on application, integration and governance," *Implement. Sci.*, vol. 19, no. 1, p. 27, Mar. 2024, doi: 10.1186/s13012-024-01357-9.

[27] W. Lv, Y. Zhao, W. Zhang, W. Liu, A. Hu, and J. Miao, "Remote measurement of short-term heart rate with narrow beam millimeter wave radar," *IEEE Access*, vol. 9, pp. 165049–165058, 2021, doi: 10.1109/ACCESS.2021.3134280.

[28] G. Beltrão, W. A. Martins, B. Shankar M. R., M. Alaee-Kerahroodi, U. Schroeder, and D. Tatarinov, "Adaptive nonlinear least squares framework for contactless vital sign monitoring," *IEEE Trans. Microw. Theory Techn.*, vol. 71, no. 4, pp. 1696–1710, Apr. 2023, doi: 10.1109/TMTT.2022.3222384.

[29] M. Xiang, W. Ren, W. Li, Z. Xue, and X. Jiang, "High-precision vital signs monitoring method using a FMCW millimeter-wave sensor," *Sensors*, vol. 22, no. 19, p. 7543, Oct. 2022, doi: 10.3390/s22197543.

[30] S. H. Oh, S. Lee, S. M. Kim, and J. H. Jeong, "Development of a heart rate detection algorithm using a non-contact Doppler radar via signal elimination," *Biomed. Signal Process. Control*, vol. 64, Feb. 2021, Art. no. 102314, doi: 10.1016/j.bspc.2020.102314.

[31] P.-L. Cheng and C.-L. Yang, "Heart rate detection with Hilbert vibration decomposition in random body movements based on FMCW radars," *IEEE Microw. Wireless Technol. Lett.*, vol. 33, no. 6, pp. 1–4, Jun. 2023, doi: 10.1109/LMWT.2023.3268347.

[32] M. Zhou, Y. Liu, S. Wu, C. Wang, Z. Chen, and H. Li, "A novel scheme of high-precision heart rate detection with a mm-wave FMCW radar," *IEEE Access*, vol. 11, pp. 85118–85136, 2023, doi: 10.1109/ACCESS.2023.3303335.

[33] H. H. Liao, W. He, and S. Y. Lin, "Heart rate evaluation algorithm based on PE-based MEEMD filter in LFMCW radar," *J. Univ. Chin. Acad. Sci.*, vol. 38, no. 5, pp. 666–677, 2021.

[34] Z. Ling, W. Zhou, Y. Ren, J. Wang, and L. Guo, "Non-contact heart rate monitoring based on millimeter wave radar," *IEEE Access*, vol. 10, pp. 74033–74044, 2022, doi: 10.1109/ACCESS.2022.3190355.

[35] Y. Hu and T. Toda, "The effect of multi-directional on remote heart rate measurement using PA-LI joint ICEEMDAN method with mm-wave FMCW radar," *IEICE Trans. Commun.*, vol. 105, no. 2, pp. 159–167, Feb. 2022.

[36] P. Zheng, C. Zheng, X. Li, H. Chen, A. Wang, and Y. Luo, "Second harmonic weighted reconstruction for non-contact monitoring heart rate," *IEEE Sensors J.*, vol. 22, no. 6, pp. 5815–5823, Mar. 2022, doi: 10.1109/JSEN.2022.3148003.

[37] M. Tazen, N. Sasaoka, and Y. Okamoto, "Non-contact heart rate measurement based on adaptive notch filter and elimination of respiration harmonics," *IEEE Access*, vol. 11, pp. 46107–46119, 2023, doi: 10.1109/ACCESS.2023.3272895.

[38] E. Antolinos, F. García-Rial, C. Hernández, D. Montesano, J. I. Godino-Llorente, and J. Grajal, "Cardiopulmonary activity monitoring using millimeter wave radars," *Remote Sens.*, vol. 12, no. 14, p. 2265, Jul. 2020, doi: 10.3390/rs12142265.

[39] Y. Ding, X. Yu, C. Lei, Y. Sun, X. Xu, and J. Zhang, "A novel real-time human heart rate estimation method for noncontact vital sign radar detection," *IEEE Access*, vol. 8, pp. 88689–88699, 2020, doi: 10.1109/ACCESS.2020.2993503.

[40] W. Lv, W. He, X. Lin, and J. Miao, "Non-contact monitoring of human vital signs using FMCW millimeter wave radar in the 120 GHz band," *Sensors*, vol. 21, no. 8, p. 2732, Apr. 2021, doi: 10.3390/s21082732.

[41] X. Huang, Z. Ju, and R. Zhang, "Real-time heart rate detection method based on 77 GHz FMCW radar," *Micromachines*, vol. 13, no. 11, p. 1960, Nov. 2022, doi: 10.3390/mi13111960.

[42] B. R. Upadhyay, A. B. Baral, and M. Torlak, "Vital sign detection via angular and range measurements with mmWave MIMO radars: Algorithms and trials," *IEEE Access*, vol. 10, pp. 106017–106032, 2022, doi: 10.1109/ACCESS.2022.3211527.

[43] B. W. Johnston, R. Barrett-Jolley, A. Krige, and I. D. Welters, "Heart rate variability: Measurement and emerging use in critical care medicine," *J. Intensive Care Soc.*, vol. 21, no. 2, pp. 148–157, May 2020, doi: 10.1177/1751143719853744.

[44] E. Mejía-Mejía, J. M. May, R. Torres, and P. A. Kyriacou, "Pulse rate variability in cardiovascular health: A review on its applications and relationship with heart rate variability," *Physiological Meas.*, vol. 41, no. 7, Aug. 2020, Art. no. 07TR01, doi: 10.1088/1361-6579/ab998c.

[45] C.-H. Chuang, J.-Y. Li, J.-T. King, W.-T. Chen, S.-P. Chen, Y.-F. Wang, H.-Y. Liu, F.-J. Hsiao, L.-L.-H. Pan, S.-J. Wang, and K.-L. Lai, "Abnormal heart rate variability and its application in predicting treatment efficacy in patients with chronic migraine: An exploratory study," *Cephalalgia*, vol. 43, no. 10, Oct. 2023, Art. no. 03331024231206781, doi: 10.1177/03331024231206781.

[46] J. Sun, Y. Yu, and L. Xin, "Research on path planning of AGV based on improved ant colony optimization algorithm," in *Proc. 33rd Chin. Control Decis. Conf. (CCDC)*, May 2021, pp. 7567–7572, doi: 10.1109/CCDC52312.2021.9601807.

[47] A. Rita Antunes, J. P. Silva, A. Cristina Braga, and J. Gonçalves, "Feature selection optimization for heart rate variability," in *Proc. 11th Int. Symp. Digit. Forensics Security (ISDFS)* May 2023, pp. 1–6.

[48] M. R. Esco, H. N. Williford, A. A. Flatt, T. J. Freeborn, and F. Y. Nakamura, "Ultra-shortened time-domain HRV parameters at rest and following exercise in athletes: An alternative to frequency computation of sympathovagal balance," *Eur. J. Appl. Physiol.*, vol. 118, no. 1, pp. 175–184, Jan. 2018, doi: 10.1007/s00421-017-3759-x.

MU LI is currently working as a Graduate Instructor with the School of Automation, Xi'an University of Technology, where he is also working as a Senior Engineer with the Engineering Training Center. His research interests include radar vital signs detection and radar signal processing.

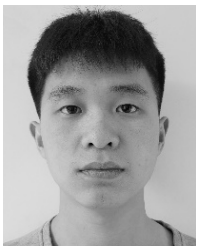

YANGYANG YANG received the bachelor's degree in electronic information engineering from Shanxi University, China, in 2022. He is currently pursuing the M.S. degree in engineering with Xi'an University of Technology, China. His research interests include vital signs algorithms and embedded systems.

XIZHENG KE received the B.S. degree in electrical engineering from Shaanxi Institute of Technology, China, in 1983, and the Ph.D. degree from the Graduate School, University of Chinese Academy of Sciences, China, in 1996. He is currently working as a Professor and the Ph.D. Supervisor with Xi'an University of Technology. His research interests include wireless laser communication theory and technology.